Establishment of a robust single axis of cell polarity by coupling of multiple positive feedback loops

Tina Freisinger, Ben Klünder, Jared Johnson, Nikola Müller, Garwin Pichler, Gisela Beck, Michael Costanzo, Charles Boone, Richard A. Cerione, Erwin Frey* and Roland Wedlich-Söldner

Supplementary Information

1. Supplementary Figures

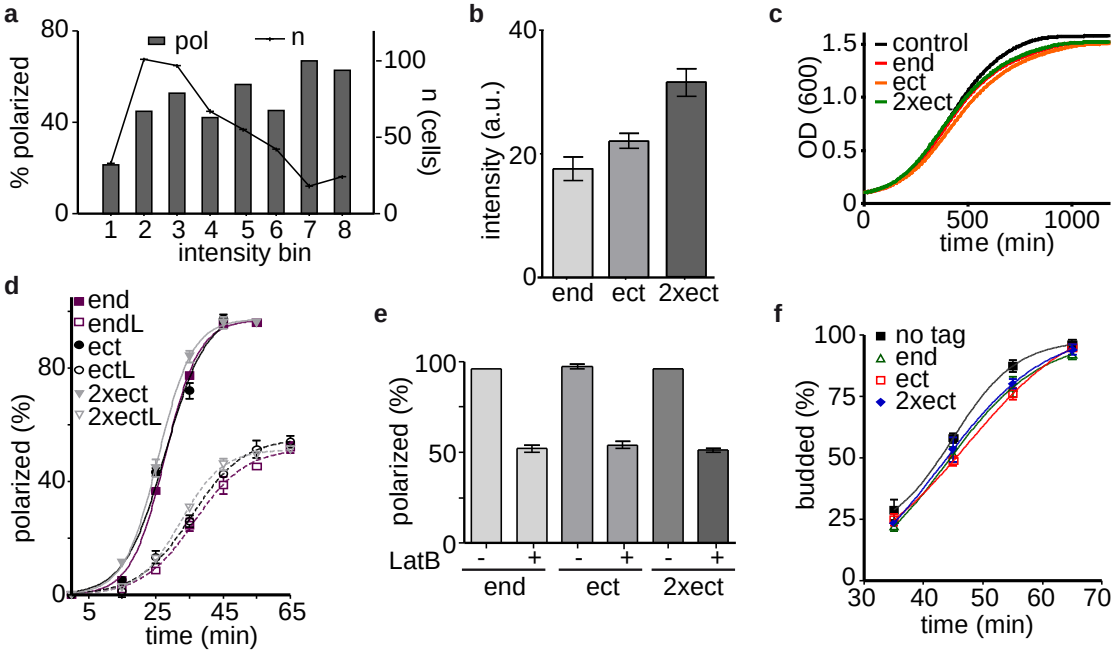

Supplementary Figure S1. Effects of Cdc42 expression level on cell polarization.

(**a**) No correlation is seen between GFP-Cdc42 expression levels (intensity bins represent ranges of relative GFP fluorescence intensity) and polarization efficiency. The number of cells analyzed for each bin is indicated (axis on the right). Levels of GFP-Cde42 were varied by inducing expression of a *GFP-CDC42* construct driven by the *GAL1* promoter for 0.5-3 h as in [30]. Number of cells (n) shown in graph. (**b**) Fluorescence intensities of cells expressing GFPCdc42 inserted at the endogenous locus (end, 1 copy), at a single ectopic site (ect; two *CDC42* copies but only one with GFP) or at two ectopic sites (2xect, three copies but only two with GFP). Values represent mean ± s.e.m. of 8 plate reader runs with > 1500 cells each. (**c**) Growth curves (average curves from three experiments shown) for control cells and cells expressing GFP-Cdc42 as indicated in (b). (**d, e)** Kinetics (d) and efficiency (e) of Cdc42 polarization in strains used in (b) and control cells after release from G1 arrest in the absence or presence of LatB. (**f**) Kinetics of bud formation in strains as indicated in (c). In (d-f) measurements represent mean ± s.d. for three experiments with n = 50 cells each.

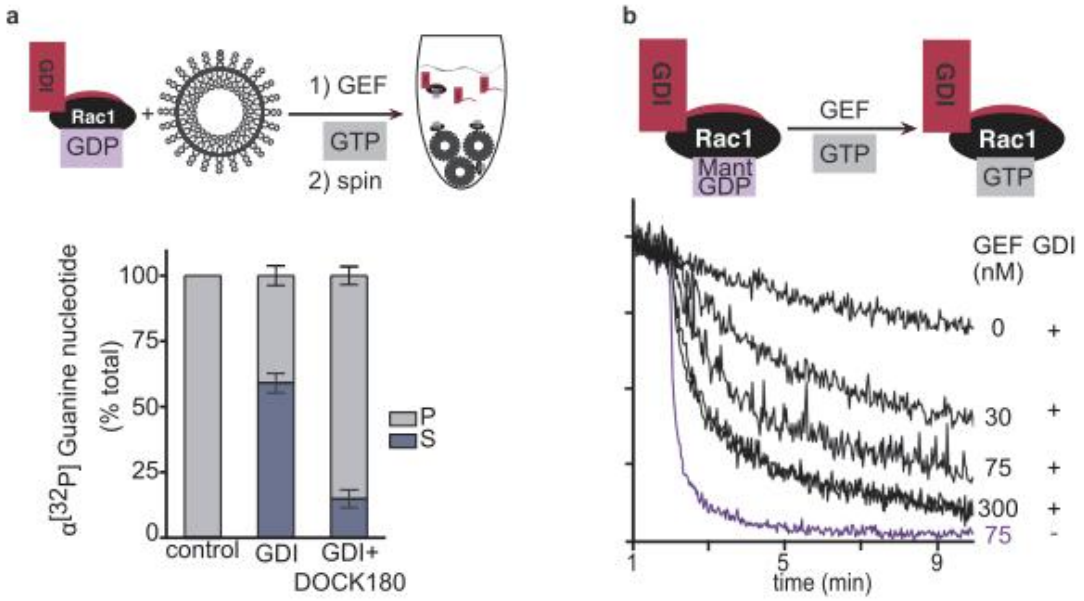

Supplementary Figure S2. Competition between GEF and GDI for GTPase binding.

(**a**) Schematic depiction (top) and result (bottom) of liposome pelleting assay. Addition of the Rac1-GEF DOCK180 blocks GDI-mediated extraction of Rac1 from liposomes. Amounts of radioactively labeled Rac1 were measured in pellet (P) and soluble (S) fractions after addition of GDI with or without the GEF domain of Dock180 (DHR2C). (**b**) Schematic depiction (top) and result (bottom) of the GDP exchange assay. The GDI inhibits nucleotide exchange. Rac1 was preloaded with Mant-GDP in the presence of liposomes, unlabelled GTP and GDI. Loss of Mant fluorescence due to nucleotide exchange was monitored after addition of the DHR2C GEF domain at 2 min. The exchange curve without added GDI is shown in purple. See **Supplementary Methods** for details.

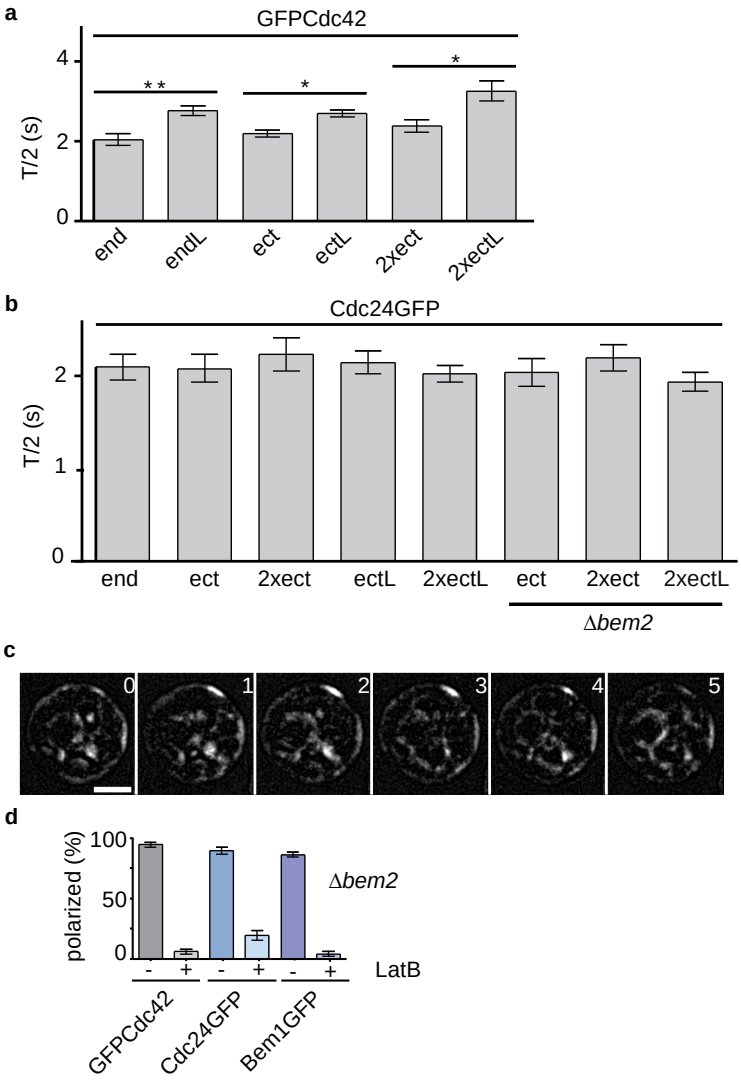

Supplementary Figure S3. Turnover of Cdc42 and Cdc24 in polarized caps.
(**a**) T/2 of GFP-Cdc42 recovery after photobleaching of polar caps in cells expressing 1-3 copies of Cdc42 (see **Supplementary Fig. S1b**) with (endL,n = 11; ectL, n = 24; 2xectL, n = 12) and without (end, n = 24; ect,n = 56; 2xect, n = 10) LatB treatment. Bars represent means ± s.e.m.. Significant ($p<0.05$, *) and highly significant ($p<0.01$, **) differences are indicated (unpaired t-test with Welsh correction). (**b**) T/2 of Cdc24-GFP in polar caps in cells expressing 1-3 copies of Cdc24 (endogenously tagged or ectopically integrated copies). Recovery values (means ± s.e.m.) are shown for control cells (n [end] = 10; n [ect] = 20; n [2xect] = 11) , cells treated with LatB ([ectL] = 14; n [2xectL] = 17), and Δ*bem2* cells (n [ect] = 10; n [2xect] = 10; n [2xectL] = 11). (**c**) An unstable GFP-Cdc42 cap in a cell exposed to LatB. Time is indicated in min. Scale bar: 4 µm. Images were subjected to background subtraction and Gaussian smoothing in ImageJ. (**d**) Bar graphs showing loss of polarization in Δ*bem2* cells treated or non-treated with LatB and expressing the indicated polarity marker. Bars correspond to mean ± s.d. of 3 experiments with 50 cells each.

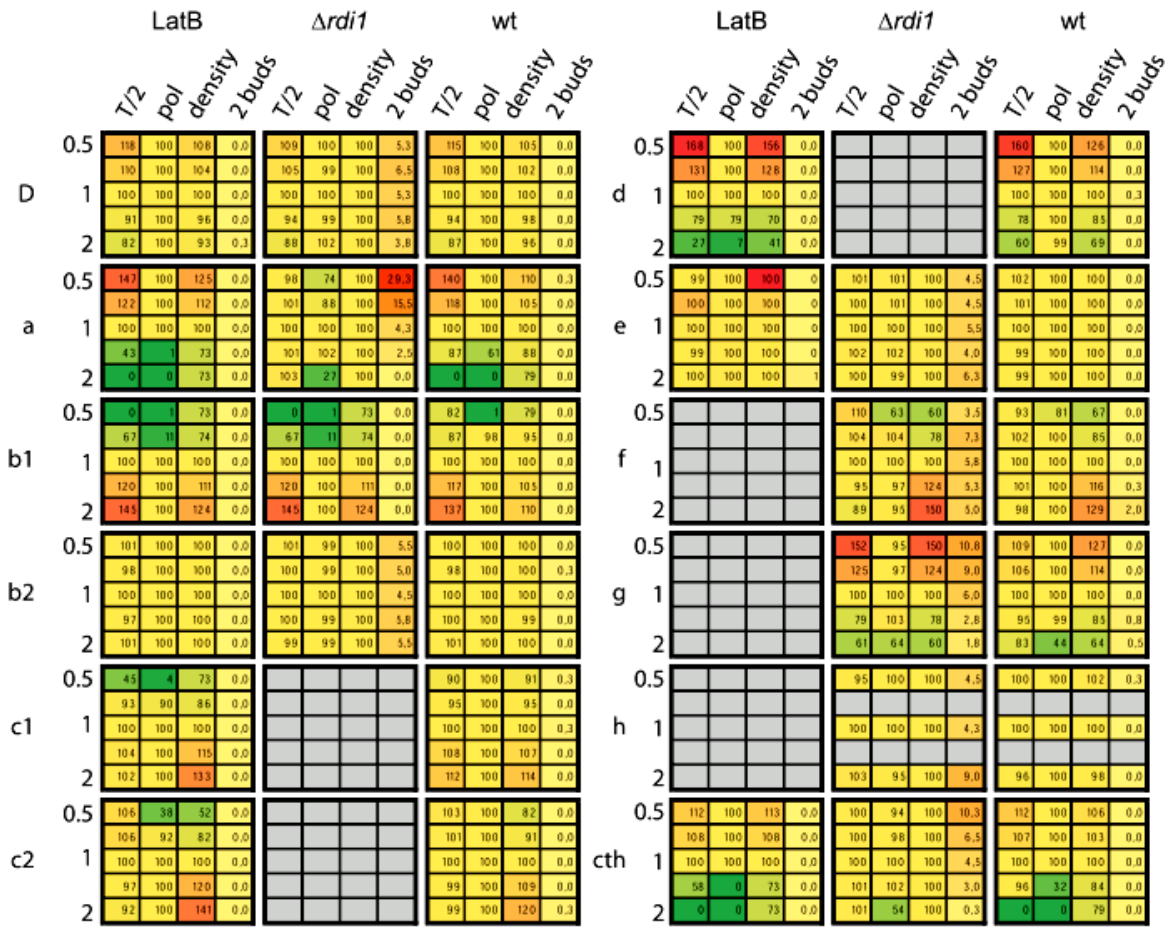

Supplementary Figure S4: Results of the parameter scan. Shown are the changes in various readouts (T/2: FRAP recovery halftime, pol: polarization efficiency, density: average Cdc42 density on plasma membrane, 2 buds: number of cells forming two buds) upon changing key parameters in our models between 2 and 0.5 fold. Parameters that are varied are indicated left of the respective matrices. For each parameter the scan results are shown for cells without actin (LatB), without the GDI (Δ*rdi1*) or for control cells (wt). For the columns "T/2", "pol" and "density" all values are shown in % of the original parameter value (1). For the column "2 buds" the actual percentage of cells with double buds is shown. Color coding: greens indicate lower values, red/dark orange indicate higher values. Yellow/light orange indicate little change compared to the original parameter value.

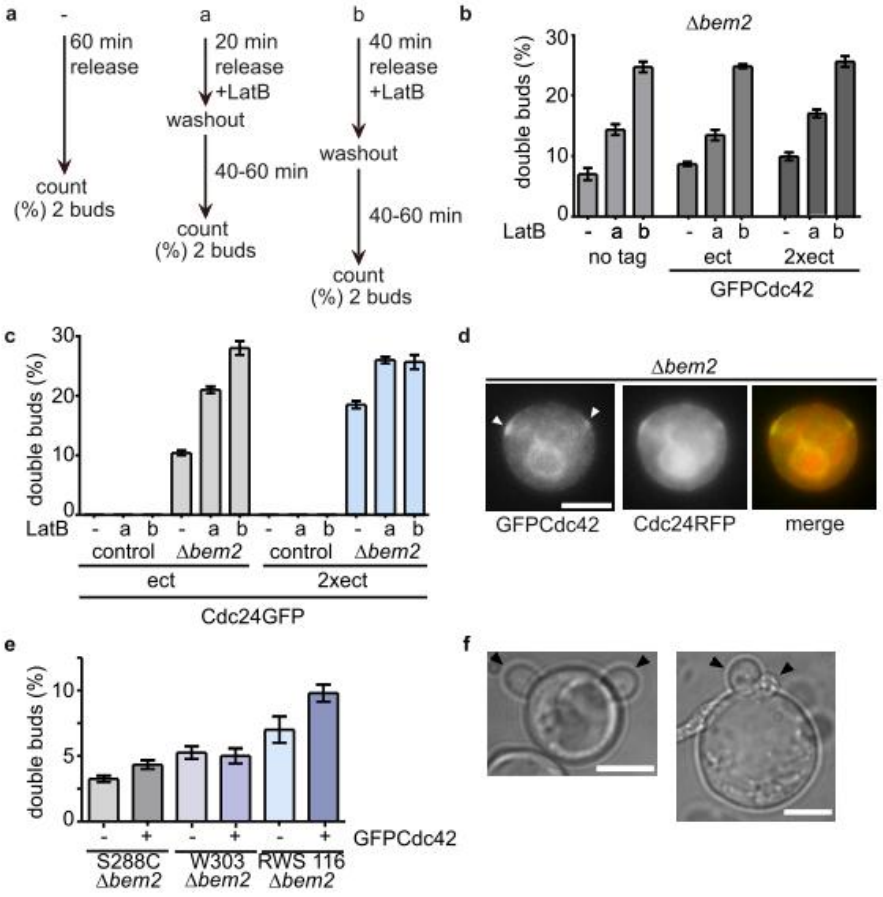

Supplementary Figure S5. Formation of multiple polarization sites.

(**a**) Schematic representation of LatB washout procedure. (**b**) Effect of prior exposure to LatB (conditions for -, a and b as in (a)) on percentage of cells with two buds formed by a Δ*bem2* strain expressing one (no tag), two (GFP-Cdc42) or three (2xGFP-Cdc42) copies of *CDC42*. Buds counted 60 min after removal of LatB. (**c**) Effect of prior exposure to LatB (conditions for -, a and b as in (a)) on the percentage of cells with two buds formed by control and *bem2Δ* strains expressing two (Cdc24-GFP) or three (2xCdc24-GFP) copies of *CDC24*. Buds counted 60 min after removal of LatB. (**d**) Colocalization of GFP-Cdc42 (green in merge) and Cdc24-RFP (red in merge) in two caps (arrowheads) in a Δ*bem2* cell. (**e**) Bar diagram showing the number of double budded cells (in percent) in synchronized cells (RWS116) or cycling cells (S288C, W303) where the Cdc42 GAP *BEM2* has been deleted. Numbers are shown for untransformed cells ("-") or cells expressing GFP-Cdc42 from a plasmid ("+", GM-Cdc42, RWC108). (**f**) Two examples of double-budded W303 Δ*bem2* cells. Bars in (b), (c) and (e) represent mean ± s.d. from at least three experiments with >100 cells each (data for (b) and (c) in **Supplementary Table S4**). Scale bars 4 µm.

2. Supplementary Tables

Supplementary Table S1. Genetic interactions*

Query	Interactor	Experiment	Interactor Category
BEM1	RSR1	(This study)	CDC42 SIGNALING
BEM1	VPS9	(This study)	ENDOCYTIC RECYCLING
RDI1	GOS1	(This study)	EARLY SECRETION
BEM2	RDI1	(This study)	CDC42 Module
CDC42	MSB3	SYNTHETIC GROWTH DEFECT	LATE SECRETION
CDC42	CAP1	SYNTHETIC GROWTH DEFECT	ENDOCYTIC RECYCLING
CDC42	BUD6	SYNTHETIC GROWTH DEFECT	ACTIN GENERAL
CDC42	GIC2	SYNTHETIC GROWTH DEFECT	CDC42 SIGNALING
CDC42	CAP2	SYNTHETIC GROWTH DEFECT	ACTIN GENERAL
BEM2	PXL1	SYNTHETIC GROWTH DEFECT	ACTIN GENERAL
CLA4	RGA1	SYNTHETIC GROWTH DEFECT	CDC42 Module
CLA4	RGA2	SYNTHETIC GROWTH DEFECT	CDC42 Module
BEM2	GET2	SYNTHETIC GROWTH DEFECT	EARLY SECRETION
BEM2	GET1	SYNTHETIC GROWTH DEFECT	EARLY SECRETION
BEM2	BEM3	SYNTHETIC GROWTH DEFECT	CDC42 Module
CLA4	RVS161	SYNTHETIC GROWTH DEFECT	ACTIN GENERAL
CLA4	PEA2	SYNTHETIC GROWTH DEFECT	ACTIN GENERAL
RGA1	RIC1	SYNTHETIC GROWTH DEFECT	ENDOCYTIC RECYCLING
CLA4	RVS167	SYNTHETIC GROWTH DEFECT	ACTIN GENERAL
CLA4	ICE2	SYNTHETIC GROWTH DEFECT	EARLY SECRETION
CDC42	SPA2	SYNTHETIC GROWTH DEFECT	ACTIN GENERAL
CDC42	RSR1	SYNTHETIC GROWTH DEFECT	CDC42 SIGNALING
CLA4	CHS6	SYNTHETIC GROWTH DEFECT	LATE SECRETION
CLA4	CHS5	SYNTHETIC GROWTH DEFECT	LATE SECRETION
BEM1	ACT1	SYNTHETIC HAPLOINSUFFICIENCY	ACTIN GENERAL
BEM2	ACT1	SYNTHETIC HAPLOINSUFFICIENCY	ACTIN GENERAL
BEM2	SMY1	SYNTHETIC LETHALITY	LATE SECRETION
CLA4	CHS5	SYNTHETIC LETHALITY	LATE SECRETION
CLA4	SMY1	SYNTHETIC LETHALITY	LATE SECRETION
CLA4	EDE1	SYNTHETIC LETHALITY	ENDOCYTIC RECYCLING
CLA4	CHS6	SYNTHETIC LETHALITY	LATE SECRETION
CLA4	BNI1	SYNTHETIC LETHALITY	ACTIN GENERAL
CLA4	BEM4	SYNTHETIC LETHALITY	CDC42 SIGNALING
CLA4	ARP2	SYNTHETIC LETHALITY	ACTIN GENERAL
BEM1	BBC1	SYNTHETIC LETHALITY	ACTIN GENERAL
BEM2	TPM1	SYNTHETIC LETHALITY	ACTIN GENERAL
CLA4	BUD6	SYNTHETIC LETHALITY	ACTIN GENERAL
CLA4	RVS167	SYNTHETIC LETHALITY	ACTIN GENERAL
CLA4	RVS161	SYNTHETIC LETHALITY	ACTIN GENERAL
CLA4	VAC14	SYNTHETIC LETHALITY	ENDOCYTIC RECYCLING
BEM2	CHS5	SYNTHETIC LETHALITY	LATE SECRETION
CLA4	SPA2	SYNTHETIC LETHALITY	ACTIN GENERAL
CLA4	MYO2	SYNTHETIC LETHALITY	LATE SECRETION
BEM2	SAC6	SYNTHETIC LETHALITY	ACTIN GENERAL
CLA4	FAB1	SYNTHETIC LETHALITY	ENDOCYTIC RECYCLING
BEM2	MYO2	SYNTHETIC LETHALITY	LATE SECRETION
BEM1	ARP2	SYNTHETIC LETHALITY	ACTIN GENERAL
CLA4	PEA2	SYNTHETIC LETHALITY	ACTIN GENERAL

CDC42	PEA2	SYNTHETIC LETHALITY	ACTIN GENERAL
CDC24	SEC15	SYNTHETIC LETHALITY	LATE SECRETION
CDC42	MSB3	SYNTHETIC LETHALITY	LATE SECRETION
CDC42	SEC10	SYNTHETIC LETHALITY	LATE SECRETION
CDC42	RSR1	SYNTHETIC LETHALITY	CDC42 SIGNALING
BEM1	BNI1	SYNTHETIC LETHALITY	ACTIN GENERAL
CDC42	BUD6	SYNTHETIC LETHALITY	ACTIN GENERAL
CDC42	BEM4	SYNTHETIC LETHALITY	CDC42 SIGNALING
CDC42	BNI1	SYNTHETIC LETHALITY	ACTIN GENERAL
CDC42	GIC2	SYNTHETIC LETHALITY	CDC42 SIGNALING
CDC42	CAP2	SYNTHETIC LETHALITY	ACTIN GENERAL
CDC42	SEC8	SYNTHETIC LETHALITY	LATE SECRETION
CDC42	SEC66	SYNTHETIC LETHALITY	EARLY SECRETION
CDC42	SEC5	SYNTHETIC LETHALITY	LATE SECRETION
CLA4	ARC40	SYNTHETIC LETHALITY	ACTIN GENERAL
CDC42	SPA2	SYNTHETIC LETHALITY	ACTIN GENERAL
CDC42	SEC9	SYNTHETIC LETHALITY	LATE SECRETION
CDC42	SEC2	SYNTHETIC LETHALITY	LATE SECRETION
CDC42	SEC15	SYNTHETIC LETHALITY	LATE SECRETION
CDC42	CAP1	SYNTHETIC LETHALITY	ENDOCYTIC RECYCLING
CDC24	BEM4	SYNTHETIC LETHALITY	CDC42 SIGNALING
CDC42	SEC3	SYNTHETIC LETHALITY	LATE SECRETION
CDC42	SEC4	SYNTHETIC LETHALITY	LATE SECRETION
BEM2	BNI1	SYNTHETIC LETHALITY	ACTIN GENERAL
BEM2	ARC40	SYNTHETIC LETHALITY	ACTIN GENERAL
RGA1	RIC1	SYNTHETIC LETHALITY	ENDOCYTIC RECYCLING
BEM2	CDC24	SYNTHETIC LETHALITY	CDC42 Module
BEM2	RGA1	SYNTHETIC LETHALITY	CDC42 Module
BEM2	ARP2	SYNTHETIC LETHALITY	ACTIN GENERAL
BEM2	CLA4	SYNTHETIC LETHALITY	CDC42 Module
BEM1	ARC40	SYNTHETIC LETHALITY	ACTIN GENERAL
BEM1	CDC42	SYNTHETIC LETHALITY	CDC42 Module
BEM1	CDC24	SYNTHETIC LETHALITY	CDC42 Module
BEM1	BEM2	SYNTHETIC LETHALITY	CDC42 Module
BEM2	ACT1	SYNTHETIC LETHALITY	ACTIN GENERAL
BEM1	SMY1	SYNTHETIC LETHALITY	LATE SECRETION
BEM1	CLA4	SYNTHETIC LETHALITY	CDC42 Module
BEM3	CDC24	SYNTHETIC LETHALITY	CDC42 Module
CDC24	CDC42	SYNTHETIC LETHALITY	CDC42 Module
CDC42	CLA4	SYNTHETIC LETHALITY	CDC42 Module
BEM1	MYO2	SYNTHETIC LETHALITY	LATE SECRETION
CDC24	CDC42	SYNTHETIC LETHALITY (CONDITIONAL)	CDC42 Module
BEM1	RDI1	[33]	CDC42 Module
BEM1	CDC42	[33]	CDC42 Module
BEM1	BOI1	[33]	CDC42 SIGNALING
BEM1	CAP2	[33]	ACTIN GENERAL
BEM1	CHS6	[33]	LATE SECRETION
CDC42	SRO7	[33]	LATE SECRETION
CDC42	TPM1	[33]	ACTIN GENERAL
BEM1	ACT1	[33]	ACTIN GENERAL
CLA4	RGA1	[33]	CDC42 Module
BEM1	BEM4	[33]	CDC42 SIGNALING
CDC42	SPA2	[33]	ACTIN GENERAL

BEM1	AIP1	[33]	ACTIN GENERAL
BEM2	CLA4	[33]	CDC42 Module
CDC42	GIC2	[33]	CDC42 SIGNALING
BEM3	RGA1	[33]	CDC42 Module
BEM2	RGA1	[33]	CDC42 Module
BEM1	BUD6	[33]	ACTIN GENERAL
BEM2	BEM3	[33]	CDC42 Module
CDC42	CAP1	[33]	ENDOCYTIC RECYCLING
BEM1	ARC18	[33]	ACTIN GENERAL
BEM1	CAP1	[33]	ENDOCYTIC RECYCLING
BEM2	CDC42	[33]	CDC42 Module
CDC42	CAP2	[33]	ACTIN GENERAL
CLA4	SHE4	[33]	LATE SECRETION
RDI1	YCK2	[33]	ENDOCYTIC RECYCLING
CLA4	RVS161	[33]	ACTIN GENERAL
RDI1	VRP1	[33]	ACTIN GENERAL
BEM1	ARF1	[33]	EARLY SECRETION
CLA4	PEA2	[33]	ACTIN GENERAL
CLA4	CHS5	[33]	LATE SECRETION
RGA1	ACT1	[33]	ACTIN GENERAL
BEM1	ARF3	[33]	ENDOCYTIC RECYCLING
CLA4	YEL1	[33]	ENDOCYTIC RECYCLING
CLA4	TPM1	[33]	ACTIN GENERAL
RDI1	TOS2	[33]	CDC42 SIGNALING
RDI1	BEM4	[33]	CDC42 SIGNALING
RDI1	PEA2	[33]	ACTIN GENERAL
CLA4	SMY1	[33]	LATE SECRETION
CLA4	SLA1	[33]	ACTIN GENERAL
CLA4	SPA2	[33]	ACTIN GENERAL
RDI1	VPS27	[33]	ENDOCYTIC RECYCLING
RGA1	SRO7	[33]	LATE SECRETION
CLA4	BUD6	[33]	ACTIN GENERAL
CLA4	CAP2	[33]	ACTIN GENERAL
CLA4	CAP1	[33]	ENDOCYTIC RECYCLING
RGA2	GET1	[33]	EARLY SECRETION
CLA4	BEM4	[33]	CDC42 SIGNALING
RGA1	VPS9	[33]	ENDOCYTIC RECYCLING
RGA1	VRP1	[33]	ACTIN GENERAL
RGA1	BUD14	[33]	ACTIN GENERAL
BEM1	ATG8	[33]	EARLY SECRETION
CLA4	EDE1	[33]	ENDOCYTIC RECYCLING
RGA1	CMD1	[33]	ACTIN GENERAL
CLA4	ICE2	[33]	EARLY SECRETION
RGA1	SLA1	[33]	ACTIN GENERAL
RGA1	SLY41	[33]	EARLY SECRETION
BEM1	BBC1	[33]	ACTIN GENERAL
CLA4	CHS6	[33]	LATE SECRETION
BEM2	CCZ1	[33]	ENDOCYTIC RECYCLING
BEM2	BUL1	[33]	ENDOCYTIC RECYCLING
BEM2	BUD6	[33]	ACTIN GENERAL
BEM2	BUD14	[33]	ACTIN GENERAL
BEM2	CCZ1	[33]	ENDOCYTIC RECYCLING
BEM2	CAP2	[33]	ACTIN GENERAL

BEM2	CAP1	[33]	ENDOCYTIC RECYCLING
BEM2	BST1	[33]	EARLY SECRETION
BEM2	APL1	[33]	ENDOCYTIC RECYCLING
BEM2	ACT1	[33]	ACTIN GENERAL
BEM1	SEC61	[33]	LATE SECRETION
BEM2	BNI1	[33]	ACTIN GENERAL
BEM2	ARF1	[33]	EARLY SECRETION
BEM2	APS2	[33]	ENDOCYTIC RECYCLING
CDC24	RIC1	[33]	ENDOCYTIC RECYCLING
BEM1	FAR10	[33]	CDC42 SIGNALING
BEM1	GIC1	[33]	CDC42 SIGNALING
BEM2	GCS1	[33]	EARLY SECRETION
BEM2	MYO2	[33]	LATE SECRETION
BEM2	ICE2	[33]	EARLY SECRETION
BEM2	GIC1	[33]	CDC42 SIGNALING
BEM2	ERV14	[33]	EARLY SECRETION
BEM2	CLC1	[33]	ENDOCYTIC RECYCLING
BEM2	CHS6	[33]	LATE SECRETION
BEM2	CHS5	[33]	LATE SECRETION
BEM2	COG7	[33]	EARLY SECRETION
BEM2	COG6	[33]	EARLY SECRETION
BEM2	CMD1	[33]	ACTIN GENERAL
BEM1	RVS167	[33]	ACTIN GENERAL
BEM1	RVS161	[33]	ACTIN GENERAL
BEM1	RUD3	[33]	EARLY SECRETION
BEM1	SEC3	[33]	LATE SECRETION
BEM1	SEC15	[33]	LATE SECRETION
BEM1	SEC10	[33]	LATE SECRETION
BEM1	KES1	[33]	EARLY SECRETION
BEM1	PEA2	[33]	ACTIN GENERAL
BEM1	MYO2	[33]	LATE SECRETION
BEM1	KIN1	[33]	LATE SECRETION
BEM1	RHB1	[33]	EARLY SECRETION
BEM1	RGP1	[33]	ENDOCYTIC RECYCLING
BEM1	PXL1	[33]	ACTIN GENERAL
BEM1	YPT31	[33]	LATE SECRETION
BEM1	VPS74	[33]	EARLY SECRETION
BEM1	VPS51	[33]	ENDOCYTIC RECYCLING
BEM1	VPS17	[33]	ENDOCYTIC RECYCLING
BEM1	YEL1	[33]	ENDOCYTIC RECYCLING
BEM1	VRP1	[33]	ACTIN GENERAL
BEM1	GIC2	[33]	CDC42 SIGNALING
BEM1	TPM1	[33]	ACTIN GENERAL
BEM1	SHE4	[33]	LATE SECRETION
BEM1	SEC72	[33]	EARLY SECRETION
BEM1	SEC63	[33]	LATE SECRETION
BEM1	SYT1	[33]	LATE SECRETION
BEM1	SPA2	[33]	ACTIN GENERAL
BEM1	SMY1	[33]	LATE SECRETION
CDC24	CAP2	[33]	ACTIN GENERAL
CDC24	CAP1	[33]	ENDOCYTIC RECYCLING
CDC24	BUD6	[33]	ACTIN GENERAL
CDC24	PEA2	[33]	ACTIN GENERAL

CDC24	GIC2	[33]	CDC42 SIGNALING
CDC24	COG7	[33]	EARLY SECRETION
CDC24	BEM4	[33]	CDC42 SIGNALING
BEM3	EDE1	[33]	ENDOCYTIC RECYCLING
BEM3	CHS5	[33]	LATE SECRETION
BEM2	SPA2	[33]	ACTIN GENERAL
BEM3	SMY1	[33]	LATE SECRETION
BEM3	SLA1	[33]	ACTIN GENERAL
BEM3	SHE4	[33]	LATE SECRETION
CDC42	BEM4	[33]	CDC42 SIGNALING
CDC24	VPS41	[33]	ENDOCYTIC RECYCLING
CDC24	VAM7	[33]	ENDOCYTIC RECYCLING
CDC24	VAM6	[33]	ENDOCYTIC RECYCLING
CDC24	YPT7	[33]	ENDOCYTIC RECYCLING
CDC24	YPT32	[33]	LATE SECRETION
CDC24	YJL206C-A	[33]	LATE SECRETION
CDC24	VAM3	[33]	ENDOCYTIC RECYCLING
CDC24	SPA2	[33]	ACTIN GENERAL
CDC24	SNX41	[33]	ENDOCYTIC RECYCLING
CDC24	RSR1	[33]	CDC42 SIGNALING
CDC24	TPM1	[33]	ACTIN GENERAL
CDC24	TLG2	[33]	EARLY SECRETION
CDC24	SPH1	[33]	LATE SECRETION
BEM2	SHE4	[33]	LATE SECRETION
BEM2	SEC72	[33]	EARLY SECRETION
BEM2	SEC66	[33]	LATE SECRETION
BEM2	SNC2	[33]	LATE SECRETION
BEM2	SMY1	[33]	LATE SECRETION
BEM2	SHE4	[33]	LATE SECRETION
BEM2	SEC3	[33]	LATE SECRETION
BEM2	RSR1	[33]	CDC42 SIGNALING
BEM2	PXL1	[33]	ACTIN GENERAL
BEM1	ERV41	[33]	EARLY SECRETION
BEM2	SEC15	[33]	LATE SECRETION
BEM2	SEC10	[33]	LATE SECRETION
BEM2	RUD3	[33]	EARLY SECRETION
BEM3	BNI1	[33]	ACTIN GENERAL
BEM2	YCK1	[33]	ENDOCYTIC RECYCLING
BEM2	VPS74	[33]	EARLY SECRETION
BEM2	VPS51	[33]	EARLY SECRETION
BEM3	ARC15	[33]	ACTIN GENERAL
BEM2	YPT32	[33]	LATE SECRETION
BEM2	YCK2	[33]	ENDOCYTIC RECYCLING
BEM2	VPS30	[33]	ENDOCYTIC RECYCLING
BEM2	SYT1	[33]	LATE SECRETION
BEM2	SSO2	[33]	LATE SECRETION
BEM2	SSO1	[33]	LATE SECRETION
BEM2	VPS21	[33]	ENDOCYTIC RECYCLING
BEM2	VAC14	[33]	ENDOCYTIC RECYCLING
BEM2	TPM1	[33]	ACTIN GENERAL

*: only negative genetic interactions were included

Supplementary Table S2. Physical interactions

Query	Interactor	Experiment	Interactor Category
BEM1	ACT1	AFFINITY CAPTURE-WESTERN	ACTIN GENERAL
BEM1	ACT1	AFFINITY PRECIPITATION	ACTIN GENERAL
BEM1	ACT1	PHYSICAL INTERACTION	ACTIN GENERAL
BEM1	ACT1	TWO HYBRID	ACTIN GENERAL
BEM1	LAS17	AFFINITY CAPTURE-WESTERN	ACTIN GENERAL
BEM1	LAS17	PHYSICAL INTERACTION	ACTIN GENERAL
BEM2	BUD14	AFFINITY CAPTURE-MS	ACTIN GENERAL
BEM2	BUD14	PHYSICAL INTERACTION	ACTIN GENERAL
BEM2	SPA2	AFFINITY CAPTURE-MS	ACTIN GENERAL
CDC42	BNI1	PHYSICAL INTERACTION	ACTIN GENERAL
CDC42	BNI1	TWO HYBRID	ACTIN GENERAL
CLA4	ABP1	PHYSICAL INTERACTION	ACTIN GENERAL
CLA4	ABP1	TWO HYBRID	ACTIN GENERAL
CLA4	SLA2	PHYSICAL INTERACTION	ACTIN GENERAL
CLA4	SLA2	TWO HYBRID	ACTIN GENERAL
RGA1	CMD1	AFFINITY CAPTURE-MS	ACTIN GENERAL
BEM1	BOI1	AFFINITY CAPTURE-MS	CDC42 SIGNALING
BEM1	BOI1	AFFINITY PRECIPITATION	CDC42 SIGNALING
BEM1	BOI1	PCA	CDC42 SIGNALING
BEM1	BOI1	PHYSICAL INTERACTION	CDC42 SIGNALING
BEM1	BOI1	TWO HYBRID	CDC42 SIGNALING
BEM1	BOI2	AFFINITY CAPTURE-MS	CDC42 SIGNALING
BEM1	BOI2	PHYSICAL INTERACTION	CDC42 SIGNALING
BEM1	BOI2	RECONSTITUTED COMPLEX	CDC42 SIGNALING
BEM1	BOI2	TWO HYBRID	CDC42 SIGNALING
BEM1	FAR1	AFFINITY CAPTURE-WESTERN	CDC42 SIGNALING
BEM1	FAR1	AFFINITY CHROMATOGRAPHY	CDC42 SIGNALING
BEM1	FAR1	PHYSICAL INTERACTION	CDC42 SIGNALING
BEM1	FAR1	RECONSTITUTED COMPLEX	CDC42 SIGNALING
BEM1	FAR1	TWO HYBRID	CDC42 SIGNALING
BEM1	RSR1	AFFINITY CHROMATOGRAPHY	CDC42 SIGNALING
BEM1	RSR1	PHYSICAL INTERACTION	CDC42 SIGNALING
BEM1	RSR1	RECONSTITUTED COMPLEX	CDC42 SIGNALING
BEM3	BEM4	PHYSICAL INTERACTION	CDC42 SIGNALING
BEM3	BEM4	TWO HYBRID	CDC42 SIGNALING
CDC24	BEM4	PHYSICAL INTERACTION	CDC42 SIGNALING
CDC24	BEM4	TWO HYBRID	CDC42 SIGNALING
CDC24	BOI1	AFFINITY CAPTURE-MS	CDC42 SIGNALING
CDC24	BOI1	AFFINITY CAPTURE-WESTERN	CDC42 SIGNALING
CDC24	BOI2	AFFINITY CAPTURE-MS	CDC42 SIGNALING
CDC24	BOI2	AFFINITY CAPTURE-WESTERN	CDC42 SIGNALING
CDC24	BOI2	PHYSICAL INTERACTION	CDC42 SIGNALING
CDC24	FAR1	AFFINITY CAPTURE-WESTERN	CDC42 SIGNALING
CDC24	FAR1	AFFINITY PRECIPITATION	CDC42 SIGNALING
CDC24	FAR1	PHYSICAL INTERACTION	CDC42 SIGNALING
CDC24	FAR1	RECONSTITUTED COMPLEX	CDC42 SIGNALING
CDC24	FAR1	TWO HYBRID	CDC42 SIGNALING
CDC24	RSR1	AFFINITY CAPTURE-WESTERN	CDC42 SIGNALING
CDC24	RSR1	AFFINITY PRECIPITATION	CDC42 SIGNALING
CDC24	RSR1	PHYSICAL INTERACTION	CDC42 SIGNALING

CDC24	RSR1	RECONSTITUTED COMPLEX	CDC42 SIGNALING
CDC24	RSR1	TWO HYBRID	CDC42 SIGNALING
CDC24	TOS2	PHYSICAL INTERACTION	CDC42 SIGNALING
CDC24	TOS2	TWO HYBRID	CDC42 SIGNALING
CDC42	BEM4	AFFINITY CAPTURE-MS	CDC42 SIGNALING
CDC42	BEM4	PHYSICAL INTERACTION	CDC42 SIGNALING
CDC42	BEM4	TWO HYBRID	CDC42 SIGNALING
CDC42	BOI1	PHYSICAL INTERACTION	CDC42 SIGNALING
CDC42	BOI1	TWO HYBRID	CDC42 SIGNALING
CDC42	BOI2	PHYSICAL INTERACTION	CDC42 SIGNALING
CDC42	BOI2	TWO HYBRID	CDC42 SIGNALING
CDC42	FAR1	PHYSICAL INTERACTION	CDC42 SIGNALING
CDC42	FAR1	TWO HYBRID	CDC42 SIGNALING
CDC42	GIC1	AFFINITY CAPTURE-WESTERN	CDC42 SIGNALING
CDC42	GIC1	PHYSICAL INTERACTION	CDC42 SIGNALING
CDC42	GIC1	RECONSTITUTED COMPLEX	CDC42 SIGNALING
CDC42	GIC1	TWO HYBRID	CDC42 SIGNALING
CDC42	GIC2	AFFINITY CAPTURE-WESTERN	CDC42 SIGNALING
CDC42	GIC2	PHYSICAL INTERACTION	CDC42 SIGNALING
CDC42	GIC2	RECONSTITUTED COMPLEX	CDC42 SIGNALING
CDC42	GIC2	TWO HYBRID	CDC42 SIGNALING
CDC42	RSR1	AFFINITY CAPTURE-WESTERN	CDC42 SIGNALING
CDC42	RSR1	RECONSTITUTED COMPLEX	CDC42 SIGNALING
CDC42	SKM1	PHYSICAL INTERACTION	CDC42 SIGNALING
CLA4	BOI2	PHYSICAL INTERACTION	CDC42 SIGNALING
CLA4	BOI2	TWO HYBRID	CDC42 SIGNALING
CLA4	GIC1	PHYSICAL INTERACTION	CDC42 SIGNALING
CLA4	GIC1	TWO HYBRID	CDC42 SIGNALING
CLA4	GIC2	PHYSICAL INTERACTION	CDC42 SIGNALING
CLA4	GIC2	TWO HYBRID	CDC42 SIGNALING
CLA4	SKM1	AFFINITY CAPTURE-MS	CDC42 SIGNALING
RGA1	GIC2	PHYSICAL INTERACTION	CDC42 SIGNALING
RGA1	GIC2	TWO HYBRID	CDC42 SIGNALING
RGA2	RSR1	TWO HYBRID	CDC42 SIGNALING
BEM3	APL6	PHYSICAL INTERACTION	EARLY SECRETION
CLA4	SEC23	AFFINITY CAPTURE-MS	EARLY SECRETION
CDC24	ENT2	PHYSICAL INTERACTION	ENDOCYTIC RECYCLING
CDC24	ENT2	TWO HYBRID	ENDOCYTIC RECYCLING
RGA1	ENT1	AFFINITY CAPTURE-WESTERN	ENDOCYTIC RECYCLING
RGA2	ENT1	AFFINITY CAPTURE-WESTERN	ENDOCYTIC RECYCLING
BEM1	SEC10	RECONSTITUTED COMPLEX	LATE SECRETION
BEM1	SEC15	AFFINITY CAPTURE-WESTERN	LATE SECRETION
BEM1	SEC15	PHYSICAL INTERACTION	LATE SECRETION
BEM1	SEC15	RECONSTITUTED COMPLEX	LATE SECRETION
BEM1	SEC15	TWO HYBRID	LATE SECRETION
BEM1	SEC5	PCA	LATE SECRETION
BEM1	SEC5	RECONSTITUTED COMPLEX	LATE SECRETION
BEM1	SEC8	AFFINITY CAPTURE-WESTERN	LATE SECRETION
CDC24	SEC15	PHYSICAL INTERACTION	LATE SECRETION
CDC24	SEC15	TWO HYBRID	LATE SECRETION
CDC42	MSB3	RECONSTITUTED COMPLEX	LATE SECRETION
CDC42	MSB4	RECONSTITUTED COMPLEX	LATE SECRETION

CDC42	SEC3	PHYSICAL INTERACTION	LATE SECRETION
CDC42	SEC3	RECONSTITUTED COMPLEX	LATE SECRETION
CLA4	SEC23	AFFINITY CAPTURE-MS	LATE SECRETION
RGA1	MLC1	AFFINITY CAPTURE-MS	LATE SECRETION
BEM1	CDC24	AFFINITY CAPTURE-MS	CDC42 Module
BEM1	CDC24	AFFINITY CAPTURE-WESTERN	CDC42 Module
BEM1	CDC24	AFFINITY PRECIPITATION	CDC42 Module
BEM1	CDC24	PCA	CDC42 Module
BEM1	CDC24	PHYSICAL INTERACTION	CDC42 Module
BEM1	CDC24	PROTEIN-PEPTIDE	CDC42 Module
BEM1	CDC24	RECONSTITUTED COMPLEX	CDC42 Module
BEM1	CDC24	TWO HYBRID	CDC42 Module
BEM1	CDC42	AFFINITY CAPTURE-WESTERN	CDC42 Module
BEM1	CDC42	PHYSICAL INTERACTION	CDC42 Module
BEM1	CDC42	RECONSTITUTED COMPLEX	CDC42 Module
BEM1	CDC42	TWO HYBRID	CDC42 Module
BEM1	CLA4	AFFINITY CAPTURE-WESTERN	CDC42 Module
BEM1	RGA2	AFFINITY CAPTURE-MS	CDC42 Module
BEM3	CDC42	TWO HYBRID	CDC42 Module
BEM3	CLA4	PHYSICAL INTERACTION	CDC42 Module
BEM3	CLA4	TWO HYBRID	CDC42 Module
CDC24	CDC42	AFFINITY CAPTURE-WESTERN	CDC42 Module
CDC24	CDC42	AFFINITY PRECIPITATION	CDC42 Module
CDC24	CDC42	PHYSICAL INTERACTION	CDC42 Module
CDC24	CDC42	RECONSTITUTED COMPLEX	CDC42 Module
CDC24	CDC42	TWO HYBRID	CDC42 Module
CDC24	CLA4	AFFINITY CAPTURE-WESTERN	CDC42 Module
CDC24	RGA2	AFFINITY CAPTURE-MS	CDC42 Module
CDC24	RGA2	AFFINITY CAPTURE-WESTERN	CDC42 Module
CDC42	CDC24	AFFINITY CAPTURE-WESTERN	CDC42 Module
CDC42	CDC24	AFFINITY PRECIPITATION	CDC42 Module
CDC42	CDC24	PHYSICAL INTERACTION	CDC42 Module
CDC42	CDC24	RECONSTITUTED COMPLEX	CDC42 Module
CDC42	CDC24	TWO HYBRID	CDC42 Module
CDC42	CLA4	AFFINITY CAPTURE-WESTERN	CDC42 Module
CDC42	CLA4	PHYSICAL INTERACTION	CDC42 Module
CDC42	CLA4	RECONSTITUTED COMPLEX	CDC42 Module
CDC42	CLA4	TWO HYBRID	CDC42 Module
CDC42	RDI1	AFFINITY CAPTURE-WESTERN	CDC42 Module
CDC42	RDI1	AFFINITY PRECIPITATION	CDC42 Module
CDC42	RDI1	FRET	CDC42 Module
CDC42	RDI1	PHYSICAL INTERACTION	CDC42 Module
CDC42	RDI1	TWO HYBRID	CDC42 Module
CDC42	RGA1	PHYSICAL INTERACTION	CDC42 Module
CDC42	RGA1	RECONSTITUTED COMPLEX	CDC42 Module
CDC42	RGA1	TWO HYBRID	CDC42 Module
CDC42	RGA2	TWO HYBRID	CDC42 Module
CLA4	RGA1	PHYSICAL INTERACTION	CDC42 Module
CLA4	RGA1	TWO HYBRID	CDC42 Module

Supplementary Table S3. FRAP values

Strain	**N**	**T/2**	**SEM**
Cdc42 (end)	24	2.03	0.15
Cdc42 (ect)	56	2.19	0.08
Cdc42 (2xect)	10	2.32	0.16
Cdc42 (end) + LatB	11	2.77	0.12
Cdc42 (ect) + LatB	24	2.55	0.07
Cdc42 (2xect) + LatB	12	3.26	0.25
Δ*rdi1* Cdc42 (ect)	20	10.56	0.45
$Cdc42^{R66E}$	11	9.14	0.66
Δ*bem2* Cdc42 (ect)	20	6.65	0.39
Δ*bem2* Cdc42 (ect) + LatB	12	9.61	0.57
$Cdc42^{G12V}$	16	33.44	2.20
$Cdc42^{D57Y}$	16	11.93	0.68
$Cdc42^{G60A}$	11	6.76	0.40
Cdc24 (end)	10	2.12	0.14
Cdc24 (ect)	20	2.10	0.15
Cdc24 (2xect)	11	2.22	0.14
Cdc24 (ect) + LatB	14	2.17	0.12
Cdc24 (2xect) + LatB	17	2.05	0.09
Δ*bem2* Cdc24 (ect)	10	2.06	0.15
Δ*bem2* Cdc24 (2xect)	10	2.26	0.18
Δ*bem2* Cdc24 (2xect) + LatB	11	1.96	0.10

Supplementary Table S4. Double buds

Strain	LatB*	N	% 2 buds	SD
Cdc42 (ect)	/	300	0.0	0.0
	a	300	0.0	0.0
	b	300	0.7	0.6
Cdc42 (2xect)	/	500	0.0	0.0
	a	300	0.0	0.0
	b	300	0.3	0.6
Cdc42 (ect)+ Cdc24OE	/	900	0.0	0.0
	a	300	0.0	0.0
	b	300	0.0	0.0
GFP-Cdc42F28L	/	500	0.0	0.0
	a	300	0.0	0.0
	b	300	0.0	0.0
Δ*rdi1* Cdc42 (ect)	/	400	2.3	0.5
	a	300	13.0	1.0
	b	300	23.0	0.6
Δ*bem2* (no tag)	/	200	7.0	1.4
	a	300	14.0	1.5
	b	300	25.0	1.5
Δ*bem2* Cdc42 (ect)	/	600	8.7	0.8
	a	300	13.0	1.5
	b	300	25.0	0.6
Δ*bem2* Cdc42 (2xect)	/	500	9.8	1.5
	a	300	17.0	1.2
	b	300	26.0	1.5
Δ*bem2* Cdc42 (ect) + Cdc24OE	/	900	12.0	1.3
	a	300	24.0	1.5
	b	300	30.0	2.6
Δ*bem2* GFP-Cdc42F28L	/	500	25.0	1.5
	a	300	55.0	0.6
	b	300	63.0	3.1
Cdc24-GFP (ect)	/	700	0.0	0.0
	a	300	0.0	0.0
	b	300	0.0	0.0
2xCdc24-GFP (2xect)	/	700	0.0	0.0
	a	300	0.0	0.0
	b	300	0.0	0.0
Δbem2 Cdc24-GFP (ect)	/	1000	10.0	1.3
	a	300	21.0	1.0
	b	300	28.0	2.0
Δbem2 2x Cdc24-GFP (2xect)	/	600	19.0	1.5
	a	300	26.0	1.0
	b	300	26.0	2.1

* /: no washout, a: washout after 20 min LatB, b: washout after 40 min LatB

Supplementary Table S5. Yeast strains

Strain	Genotype*	Source/Reference
RWS116	MATa *cln1*::HisG *cln2*Δ *cln3*::HisG YipLac204-MET-CLN2::TRP1 *ura3 his3-11,15 ade2-1can1-100*	[60]
RWS119	pGal-myc-GFP-CDC42::URA3 (RWC108)	this study
RWS794	pCDC24-CDC24-GFP::hphNT1	this study
RWS1023	pCDC42-myc-GFP-CDC42^{D57Y}::URA3 (RWC686)	this study
RWS1024	pCDC42-myc-GFP-CDC42^{R66E}::URA3 (RWC689)	this study
RWS1028	Δ*bem2*::G418	this study
RWS1029	Δ*bem2*::G418 pCDC24-CDC24-GFP::LEU2 (RWC153)	this study
RWS1031	Δ*bem2*::G418 pCDC42-myc-GFP-CDC42::URA3 (RWC108) p42-GFP-Cdc42::LEU2 (RWC151)	this study
RWS1034	pCDC42-GFP-CDC42::cloNAT	this study
RWS1035	Δ*bem2*::G418 pCDC42-myc-GFP-CDC42::URA3 (RWC108)	this study
RWS1036	pCDC42-myc-GFP-CDC42^{G60A}::URA3 (RWC688)	this study
RWS1037	pCDC42-myc-GFP-CDC42^{G12V}::URA3 (RWC687)	this study
RWS1038	Δ*vps27*::G418 pCDC42-myc-GFP-CDC42::URA3 (RWC108)	this study
RWS1039	Δ*rdi1*::LEU2 Δ*vps27*::G418 pCDC42-myc-GFP-CDC42::URA3 (RWC108)	this study
RWs1040	pCDC24-CDC24-GFP::LEU2 (RWC153) pCDC24-CDC24-GFP::URA(RWC146)	this study
RWS1041	Δ*bem2*::G418 pCDC24-CDC24-GFP::LEU2 (RWC153) pCDC24-CDC24-GFP::URA(RWC146)	this study
RWS1047	*myo2-16* pCDC42-myc-GFP-CDC42::URA3 (RWC108)	this study
RWS1048	*myo2-16* Δ*rdi1*::LEU2 pCDC42-myc-GFP-CDC42::URA3 (RWC108)	this study
RWS1088	pCDC42-myc-GFP-CDC42::URA(RWC108) pCdc24Cdc24mRFP-Ruby::LEU2 (RWC723)	this study
RWS1099	pCDC42-myc-GFP-CDC42::URA3(RWC108) p42-GFP-Cdc42::LEU2 (RWC151)	this study
RWS1135	pCDC42-myc-GFP-CDC42^{F28L}::URA3 (RWC790)	this study
RWS1136	Δ*bem2*::G418 pCDC42-myc-GFP-CDC42^{F28L}::URA3 (RWC790)	this study
RWS1421	pCDC42-myc-GFP-CDC42::URA3 (RWC108)	this study
RWS1422	pCDC24-CDC24::LEU2 (RWC153)	this study
RWS1423	Δ*rdi1*::LEU2 pCDC42-myc-GFP-CDC42::URA3 (RWC108)	this study
RWS1424	Δ*bem2*::G418 pCDC42-myc-GFP-CDC42::URA(RWC108) pCdc24Cdc24mRFP-Ruby::LEU2 (RWC723)	this study

*all strains were made in the RWS 116 background

Supplementary Table S6. Plasmids

Plasmid	Origin	Description	Source/Reference
RWC21	pRS306	GFP-CDC42 under the control of Gal promoter in a pRS306 backbone for integration into the URA3 locus after linearization	[14]
RWC108	pRS306	GFP-CDC42 under the control of the endogenous CDC42-promoter in a pRS306 backbone for integration into the URA3 locus after linearization	[14]
RWC146	pRS316	CDC24-GFP under the control of the endogenous CDC24-promoter in a pRS316 backbone URA3-CEN plasmid	this study
RWC148	pRS305	pRS305 backbone for integration into the LEU2 locus after linearization	this study
RWC151	pRS305	GFP-CDC42 under the control of the endogenous CDC42-promoter in a pRS305 backbone for integration into the LEU2 locus after linearization	this study
RWC153	pRS305	CDC24-GFP under the control of the endogenous CDC24-promoter in a pRS305 backbone for integration into the LEU2 locus after linearization	[14]
RWC233	pYM-25	Plasmid for C-terminal direct tagging, hphNT1.	[56]
RWC257	pYM-N4	Plasmid for N-terminal direct tagging, clonNAT.	[56]
RWC550	pYM-N4	Plasmid for N-terminal direct tagging, clonNAT under the control of the endogenous CDC42 promoter	[56]
RWC686	pRS306	GFP-CDC42D57Y under the control of the endogenous CDC42-promoter in a pRS306 backbone for integration into the URA3 locus after linearization	this study
RWC687	pRS306	GFP-CDC42G12V CDC42D57Y under the control of the endogenous CDC42-promoter in a pRS306 backbone for integration into the URA3 locus after linearization	this study
RWC688	pRS306	GFP-CDC42G60A CDC42D57Y under the control of the endogenous CDC42-promoter in a pRS306 backbone for integration into the URA3 locus after linearization	this study
RWC689	pRS306	GFP-CDC42R66E CDC42D57Y under the control of the endogenous CDC42-promoter in a pRS306 backbone for integration into the URA3 locus after linearization	this study
RWC723	pRS305	CDC24-mRFP CDC42D57Y under the control of the endogenous CDC24-promoter in a pRS305 backbone for integration into the LEU2 locus after linearization	this study
RWC790	pRS306	GFP-CDC42F28L under the control of the endogenous CDC42-promoter in a pRS306 backbone for integration into the URA3 locus after linearization	this study

Supplementary Table S7. Primer

Primer	Sequence 5'→3'	use
RWS650	AGCAAAACTTATAAAACAAGAAATAAACGTATTAGCTCTTCCACAAAATGcgtacgctgcaggtcgac*	Cdc42 genomic GFP integration
RWS651	CACGTTTTCCCAACAGCACCATCACCGACAACAACACACTTTAGCGTTTGCatcgatgaattctctgtcg	Cdc42 genomic GFP integration
RWS618	TCCGGATTTGTGGAAGAGCTAATACGTTTATTTC	Cdc42 promoter with BspEI
RWS617	GAGCTCCAGGCCGGAACTCAAAAGG	Cdc42 promoter with SacI
RWS655	AAGAAATGTTGGCGGAAAACAATGAGAAATTCTTGAACATTCGTCTGTAT cgtacgctgcaggtcgac	Cdc24 genomic GFP integration
RWS654	GTTTTTTTCTTGAATTATTTAGTATTTGCTGTATACTAGTTTTATTTATCA atcgatgaattcgagctcg	Cdc24 genomic GFP integration
RWS347	AGGCAAGAGATCAGGCGGAAAGA	amplification of KanMX-cassette
RWS346	AGAAGCAAGCTACGTTGCAGCCA	amplification of KanMX-cassette
RWS885	CAGGTTTCATTGGAGGTGC	Bem2 deletion test primer
RWS265	GGTGCTCAACAATTCAGTTCT	Bem2 deletion test primer
RWS352	TGCACCAACATACCGTTTTGC	Bem2 deletion test primer
RWS351	TGATGGTAAATCCCGTCCTGC	Bem2 deletion test primer
RWS98	CACGGAGCCTACCTTTTAG	Vps27 deletion test primer
RWS97	GTTCGTGTGGTTAGACAAC	Vps27 deletion test primer
RWS207	TGATGCTTTGTAGCTGTTGCTC	Vps27 deletion test primer
RWS206	AGAGAAGCTGAAGAAGCGAAGC	Vps27 deletion test primer
RWS343	TGAAATGCTTCTGAGCGAAGC	Vps27 deletion test primer
RWS342	TCAAATGCCTTGCTGACCACT	Vps27 deletion test primer
RWS1112	GAGCGCAACGCAATTAATG	Cdc42 amplification from RWC 21
RWS73	CTGCCCTTTCGAAAGATC	Cdc42 amplification from RWC 21
RWS1110	GATATGACAAGGGTCTCAATTCATCGTAATCTTCTTGACCG	R66E mutation primer
RWS1109	GAAGATTACGATGAATTGAGACCCTTGTCATATC	R66E mutation primer
RWS1112	GAGCGCAACGCAATTAATG	Cdc42 amplification from RWC 21
RWS73	CTGCCCTTTCGAAAGATC	Cdc42 amplification from RWC 21
RWS1540	GGAACATAGTCGGCTGGCAATTGATTCGTTGTATAG	F28L mutation primer
RWS1539	CTATACAACGAATCAATTGCCAGCCGACTATGTTCC	F28L mutation primer
RWS48	GTATTCTGGGCCTCCATG	KanMX test primer
RWS47	GATACTAACGCCGCCATC	KanMX test primer
RWS1247	TGAGCTGCGCACGTCAAG	KanMX test primer
RWS1246	TGGTCGCTATACTGCTGTC	KanMX test primer

* restriction endonuclease sites are underlined; homology regions for direct integration are depicted in small letters

Supplementary Table S8: **Model reactions**

Reaction	Formula
Membrane diffusion	$T_i \xrightarrow{k_D} T_{i\pm1}$, $D_i \xrightarrow{k_D} D_{i\pm1}$
Hydrolysis	$T_i \xrightarrow{a} D_i$
Nucleotide exchange	$D_i \xrightarrow{b_1 T_i/(c_{th}+\sum_j T_j)+b_2} T_i$
Recruitment	$D_{cyt} \xrightarrow{c_1 T_i/(c_{th}+\sum_j T_j)} T_i$, $D_{cyt} \xrightarrow{c_2} D_i$
Extraction	$D_i \xrightarrow{d} D_{cyt}$
Actin bundle nucleation	$A_{cyt} \xrightarrow{eT_i} A_i$
Exocytosis	$T_{IM} \xrightarrow{f[A_i+(h-\sum_j A_j)/n]/h} T_i$, $D_{IM} \xrightarrow{f[A_i+(h-\sum_j A_j)/n]/h} D_i$
Endocytosis	$T_i \xrightarrow{g} T_{IM}$, $D_i \xrightarrow{g} D_{IM}$

Supplementary Table S9. Model parameters

parameter	value	description
n	100	number of lattice sites
R	3.95 μm	cell radius; from this work
D	0.036 $\mu m^2/s$	diffusion constant (Marco et al., 2007)
k_D	0.585/s	corresponding model reaction rate
N_{42}	3000	Cdc42 per cell; estimate obtained by comparing the fraction of Cdc42 in the cytosol and the total amount of GDI per cell (Ghaemmaghami et al., 2003; Wedlich-Soeldner et al., 2004)
N_A	2	number of assumed possible actin bundle nucleation sites
a	2.74/s	hydrolysis rate; fitted to provide latrunculin treated control cell properties
b_1	63.1/s	GEF-mediated nucleotide exchange rate; fitted to provide properties of LatB treated control cells
b_2	0.0002/s	intrinsic nucleotide exchange rate (Zheng et al. JBC, 1994)
c_1	0.04472/s	GEF-mediated membrane attachment rate of cytosolic Cdc42; fitted to provide properties of LatB treated control cells
c_2	0.0015/s	basal membrane attachment rate of cytosolic Cdc42; fitted to provide properties of LatB treated control cells
d	0.5/s	Cdc42-GDP extraction rate; estimated from Cdc42 FRAP in this work
e	0.000139/s	actin bundle nucleation rate; fitted to provide properties of Δ*rdi1* cells
f	0.02236/s	rate describing the total exocytosis of Cdc42 to the membrane; fitted to provide properties of Δ*rdi1* cells
h	4	parameter defining rate of background exocytosis of Cdc42; fitted to provide properties of Δ*rdi1* cells
g	0.04472/s	endocytosis rate; fitted to provide properties of Δ*rdi1* cells
c_{th}	100	threshold of bounded feedback; estimate based on the approximate amount of Cdc42 in the polarity cluster

Supplementary Table S10 Comparison of features and limitations in models for yeast cell polarity

paper	type of model	level of detail	mathematical complexity	step of polarity
Wedlich-Soldner, 2003 (ref. 13)	stochastic	conceptual	low	establishment
	Conceptual model that does not include realistic descriptions of Cdc42 diffusion or endocytosis. Biological predictions are kept very general. Only active Cdc42 is considered.			
Marco, 2007 (ref. 37)	deterministic	mechanistic	low, 1 PDE	maintenance
	Includes detailed measurements for lateral diffusion, endocytosis and secretion of Cdc42. Concludes that endocytosis is optimized for sharpness of polarization. Uses coarse-grained model for actin-mediated transport steps. Mainly considers active Cdc42.			
Goryachev, 2008 (ref. 28)	deterministic	mechanistic	high, 8 PDEs	establishment
	Reaction-diffusion system where mass conservation enforces formation of a single stable cluster from multiple intermediates by coarsening. Very detailed model of the Cdc42 GTPase cycle. Includes several biochemical parameters that are not experimentally validated, such as Cdc42-GTP-dependent GEF turnover, which does not fit our own results (see text for details).			
Altschuler, 2008 (ref.30)	stochastic	conceptual	low	establishment
	Linear positive feedback provides stochastic clustering at low protein number. Due to their stochastic nature clusters are only transient. Very simple model, which only requires a single positive feedback. Model predictions are not validated by experimental results.			
Slaughter, 2009 (ref. 17)	deterministic	mechanistic	intermediate, several PDEs	maintenance
	Combines GDI- and actin-mediated recycling pathways for Cdc42. Provides detailed measurements and parameters for uptake and delivery of Cdc42. Makes quantitative predictions. Concludes that endocytosis and GDI-mediated Cdc42 internalization are optimized for a particular shape of polarization in budding vs. mating cells. Does not consider symmetry breaking / polarity establishment.			
Howell, 2009 (ref. 46)	deterministic	mechanistic	high	maintenance
	Uses model by Goryatchev 2008 to predict formation of multiple buds through failure of competition in a reaction-diffusion system. Does not consider relevance of actin for formation of multiple buds. Ambiguous localization of chimeric constructs makes interpretation difficult (Bem1-t-SNARE fusion induces formation of multiple buds and simultaneously localizes to bud scar and cortical patches).			

paper	type of model	level of detail	mathematical complexity	step of polarity
Layton, 2011 (ref.25)	stochastic	mechanistic	high	maintenance
	Model of actin-dependent polarization of Cdc42 that explicitly considers vesicular intermediates of endo- and exocytosis. Predicts that polarization via actin cannot occur with previously measured diffusion constants for Cdc42. Introduces several parameters for endocytic recycling that have not been experimentally validated. Cannot explain formation of multiple buds. Makes simplifying assumptions on kinetics of lipids and proteins during vesicle fusion (lipids are likely to diffuse much faster, which would oppose the postulated dilution effect).			
Savage, 2012 (ref. 21)	stochastic	mechanistic	high	maintenance
	Combines models of Howell 2009 and Layton 2011. Questions the contribution of actin to Cdc42 recycling and polarity establishment. Ignores the previously documented ability of yeast cells to polarize independently of Bem1 and exclusively via actin-mediated transport. The prediction of increased Cdc42 cap intensity after treatment with LatB is not validated by our experiments (see text).			
Howell, 2012 (ref. 24)	deterministic	mechanistic	high	maintenance
	Extends model in Howell 2009 by negative feedback. Shows oscillating cortical patches. Synchronization with hydroxyurea yields cells with ill-defined cell cycle stage and Cdc42 regulation. Oscillation is not observed in unpolarized, cyclin-depleted cells arrested at the G1-S transition. Does not provide explanations for double budded cells. Results can therefore not be directly compared.			
Freisinger (this work)	stochastic	mechanistic	intermediate	establishment
	First stochastic model for combined GDI and actin-mediated Cdc42 recycling. Combination of pathways confers uniqueness, speed and robustness of polarization response. Model kept as simple as possible and only includes experimentally validated parameters. Coarse graining of the actin-mediated pathway is currently necessary as more detailed parameters cannot be reliably measured.			

3. Supplementary Methods

Effects of Cdc42 expression level on polarization efficiency Fig. S1a**:** Cells expressing GM-Cdc42 (Cdc42 N-terminally tagged with GFP and Myc_6) from the *CDC42* promoter or a galactose-inducible promoter were grown overnight in SC-methionine and 2% glucose, washed three times with distilled water, diluted into SC-methionine containing 2% raffinose, and then arrested for 3 h in G1 in YPD supplemented with 2 % raffinose and 3 mM methionine. Cells expressing GM-Cdc42 from the *GAL* promoter were induced for either 30 min or 90 min by addition of 2% galactose. To disrupt the actin cytoskeleton, cells were treated with 150 µM LatA during release from G1. Polarized cells were counted after 30 min and 60 min (cells expressing GM-Cdc42 under the *CDC42* promoter) and after 30 min and 90 min (galactose-induced cells). Expression levels of GM-Cdc42 were determined by integrating fluorescence intensity for each cell.

Growth Assay Logarithmically growing cells were grown to an OD_{600} of 0.3, diluted 10 fold with medium and transferred to a 96-well flat-bottom plate (Corning). Growth rates were measured every 5 min at 30°C and $OD_{620}$with a Multiscan FC 96-well reader (Thermo Scientific). Measurements of each strain were done in triplicates. Growth curves were analysed and fitted with Prism 4.0 (Graphpad).

Fluorescent Intensity measurements Fluorescent intensities of logarithmically growing cells were measured using an INCell Analyzer 2000 (GE Healthcare) equipped with a 40x/0.6 air objective. Images of living yeast cells were automatically acquired from several positions per well with exposure times of 50 ms for the brightfield channel, 1800 ms for GFP fluorescence and 500 ms for RFP fluorescence using appropriate filter sets. 25 images with >100 cells were acquired per strain and channel and quantified using INCell Analyzer Workstation v3.7 software.

Nucleotide exchange assay Competition between GDI and the guanine nucleotide exchange factor Dock180 was measured with prenylated Rac1. Rac1 was preloaded with Mant-GDP in a 25-µl volume in the presence of 20 µl of unlabeled 1-µm liposomes. After transferring the mixture (containing 60 nM Rac1 and 500 nM Mant GDP) to the cuvette, unlabeled GTP (10 µM) and GDI (80 nM) were added for 10 min. At the indicated times, different concentrations of the DHR2 domain of Dock180 were added. Traces monitored the loss of Mant fluorescence due to nucleotide exchange.

For radioactive Rac1-liposome association assays, Rac1 (40 nM) was preloaded with α[^{32}P]GTP (2300 cpm/pmol, 10 μM) by EDTA (8 mM)-stimulated nucleotide exchange in the presence of 8 μm liposomes (1 mg/ml). Rac1 was allowed to hydrolyze bound nucleotide to α[^{32}P]GDP for 30 min on ice in presence of excess magnesium (14 mM). This also prevented further EDTA-stimulated nucleotide exchange. The protein was then incubated with 45 nM GDI for 10 min, followed by 10 min with the DHR2 domain of Dock180 (500 nM) in the presence of 100 μM unlabeled GTPγS. The mixture was pelleted for 10 min at 16,000$\times g$, and radioactivity levels in the supernatant and pellet fractions were measured.

Stochastic model of cell polarity. We built a stochastic particle-based model and simulated the emergence of polarity in budding yeast. Our model explicitly includes as variables the active (*T*) and inactive (*D*) forms of Cdc42, which can be recruited to the plasma membrane and accumulate in caps. A pool of Cdc42 (T_{IM}, D_{IM}) can be found on internal membranes (*IM*) and is allowed to shuttle between plasma membrane and internal membranes via endocytosis and exocytosis. Cdc42 can also be extracted from the plasma membrane directly into a well-mixed pool of cytosolic Cdc42-GDP (D_{cyt}) by interaction with its GDI, Rdi1. We considered a two-dimensional model of a circular shaped cell with radius *R*. The membrane was split into *n* = 100 segments where reactions take place between particles on the same segment $i = 1,\ldots,n$. This approach allowed us to stochastically simulate the temporal evolution of the system using the Gillespie algorithm[61].

We fitted our model to recapitulate the emergence of Cdc42 caps in latrunculin-treated and in Δ*rdi1* cells, and tested its reliability by comparing the predictions of the combined model with our experimental results derived from wild-type cells and mutants altered in GTP hydrolysis.

To achieve and maintain polarization, Cdc42 must be continuously returned to the cap, as diffusion in the plasma membrane acts to flatten any inhomogeneities in protein distribution. We incorporated diffusion of Cdc42 in the plasma membrane as jumps between neighbouring segments with the stochastic rate constant k_D. The rate can be calculated from $k_D = D/(2\pi R/n)^2$, where *D* is the diffusion constant and *R* the cell radius[62].

The intrinsic GDP exchange activity of Cdc42 is increased by its only GEF, Cdc24, which is delivered to already active Cdc42 on the membrane by the effector Bem1[15, 27]. However, recruitment of Cdc24 and Bem1 to the cap is bounded by limited availability of the molecules involved[14]. We employed an effective description of this bounded positive feedback such that the activation rate for the process

$$D_i \xrightarrow{b_1 F(\{T_i\})} T_i$$

is given by a Michaelis-Menten law $F(\{T_i\}) = T_i / (c_{th} + \sum_i T_i)$ with amplitude b_1. Here D_i and T_i denote the number of passive and active Cdc42 respectively at site *i*. The denominator of $F(\{T_i\})$ effectively limits GEF recruitment if the total amount of active Cdc42 substantially exceeds the threshold c_{th}. Moreover, we used a similar functional form $F(\{T_i\})$ to account for GEF-mediated recruitment of Cdc42 from the cytosol with subsequent nucleotide-exchange

$$D_{cyt} \xrightarrow{c_1 F(\{T_i\})} T_i$$

This term reflects direct or indirect competition for Cdc42 binding between GEF and GDI as shown in **Supplementary Fig. S2**. The resulting displacement of the GDI by the GEF has been suggested previously for mammalian Rho and Rab GTPases[40, 41, 52]. In the absence of GEF, nucleotide-exchange and membrane attachment of Cdc42-GDP are assumed to occur at background rates b_2 and c_2.

Direct extraction of Cdc42-GDP from the plasma membrane is facilitated by interaction with its GDI Rdi1 (Fig. 3d and[9, 17]). We assumed that Rdi1 is present in large excess and diffuses rapidly in the cytosol. Therefore the extraction of Cdc42-GDP into the well-mixed cytosolic pool of Cdc42 is taken to occur with a constant rate *d*.

Since Rdi1 preferentially interacts with Cdc42-GDP (see Fig. 3d), the last reaction necessary for Rdi1-dependent polarization is hydrolysis of Cdc42-GTP. This we implemented as a first-order reaction with rate *a*. The reactions of the Rdi1-dependent polarization pathway are shown in Fig. 3c.

A second mechanism for Cdc42 recycling and cell polarization is provided by actin-mediated transport. We were mainly interested in how the distribution of Cdc42 affected the reorganization of the cytoskeleton and heuristically modelled the effective protein dynamics induced by endocytosis and exocytosis. Details of the model are shown in Fig. 3b.

We assumed that the nucleotide bound to Cdc42 does not change during recycling as intrinsic nucleotide exchange and hydrolysis rates are very low[63] and the GAP and GEF for Cdc42 are expected to be mostly active on the plasma membrane where they are present at higher concentration in polar caps or patches[14]. Cdc42 caps are maintained by a dynamic balance of focused exocytosis, dilution by lateral diffusion within the plasma membrane, and endocytosis[37]. We made the simplifying assumption that the total exocytic flux of Cdc42 remains the same before and after polarization for a given internal pool of cargo. The flux of

Cdc42 from the internal membranes is equally spread over the whole plasma membrane in unpolarized cells but is slightly focused in polarized cells. We implemented this in our model by allowing the "nucleation" of $N_A = 2$ sites of increased exocytosis on the plasma membrane similar to earlier models[37]. As actin reorganization is under control of Cdc42-GTP we modelled the nucleation of stable actin bundles as

$$A_{cyt} \xrightarrow{eT_i} A_i$$

where A_{cyt} and A_i represent available and nucleated stable actin bundles, respectively, with $\Sigma A_i + A_{cyt} = N_A$.

The exocytic flux is described by the reactions

$$T_{IM} \xrightarrow{f[A_i+G(A_i)]/h} T_i,$$

$$D_{IM} \xrightarrow{f[A_i+G(A_i)]/h} D_i$$

with $G(\{A_i\}) = (h - \sum_i A_i)/n$, where h describes a background exocytosis rate in regions not impinged upon by actin cables. This description allows for focused exocytosis along nucleated actin bundles while keeping total exocytosis constant. Finally, we approximated endocytosis of Cdc42 to internal membranes by a constant endocytosis rate *g*.

All reactions of the agent-based model are summarized in **Supplementary Table S8**:

Parameter estimates. To fit our model we first separately considered LatB-treated control and Δ*rdi1* cells. The diffusion constant *D* of Cdc42, the total number N_{42} of Cdc42 and the intrinsic activation rate b_2 were taken or estimated from published data[14, 37, 63, 64]. The average cell radius *R* was determined to be 3.95 μm. As LatB-treated control cells show a Cdc42 mobility (FRAP) rate of approximately 0.28/s, we estimated the extraction rate *d* to be 0.5/s. As initial conditions for LatB-treated cells we distributed on average 20% of all Cdc42 to the plasma membrane, with the remaining Cdc42 being split equally between membranes and cytosol[14]. In simulations of Δ*rdi1* cells the cytosolic fraction was redistributed to the membranes, with one third being allocated to the plasma membrane. To begin our simulation, we assumed that the GEF had just arrived at the plasma membrane, and started with an average fraction of active Cdc42 on all membranes determined by the ratio of intrinsic activation and hydrolysis. The activation threshold c_{th} limiting the total amount of active GEF

was estimated to be 100, given that roughly 300 Cdc42 molecules are localized to steady-state caps[14, 64].

The remaining parameters were chosen such that the caps formed in LatB-treated and Δ*rdi1* cells satisfied a set of constraints over an average of 400 runs. We fitted the GEF-dependent activation and recruitment rates b_1 and c_1, and the hydrolysis and background insertion rates a and c_2 in LatB simulations assuming exocytosis and endocytosis to be zero. Using previous FRAP and fractionation results[14] we estimated the fraction of Cdc42 in the cap at steady state to be 10%, with the same amount being distributed over the rest of the plasma membrane. From our data shown here (Fig. 4) and previous publications[17, 37] we estimated the height and width of Cdc42 caps to 10 times the background density and 10% of the circumference, respectively.

The fitting constraints were a Cdc42 FRAP time in steady-state LatB caps of 2-3 s, a total amount of Cdc42 on the plasma membrane of 15-25%, a cap height of 7-12 times the background, and a cap width of 8-12%. Each simulation was terminated after t_{end} = 1300 s internal simulation time - comparable to the duration of our experiments and the time cells take to polarize after GEF release from the nucleus[50, 65]. A cap was deemed to have formed if a spatially averaged profile of Cdc42 (over 5% of the membrane) was higher than twice its average value. At the end of the simulation the number of caps and the particle density of Cdc42 were determined and a Gaussian distribution was fitted to the Cdc42 profile to quantify its shape. We defined the cap width as twice the distance between the turning points of the fit.

To simulate FRAP values, at time t_{frap} = 1200 s the number of caps was determined. For simulations with a single cap, Cdc42 in a region corresponding to 20% of the plasma membrane and centred at the cap position was changed into a "non-fluorescent" version of Cdc42. The migration of fluorescent Cdc42 into the cap was then monitored and the recovery halftime T/2 was calculated by fitting with a single exponential function.

After fitting the model to LatB-treated cells we used the parameters obtained and successively fitted the actin nucleation rate e, the exocytosis parameters f and h, and the endocytosis rate g for Δ*rdi1* cells. Model parameters for Δ*rdi1* cells were chosen such that steady-state caps had a FRAP recovery time of 10-12 s, with 30-40% of all Cdc42 on the plasma membrane, a cap height of 7-12 times background, 0-10% cells with double caps and 90-100% total polarization. For LatB-treated cells we obtained 19% of all Cdc42 on the plasma membrane, 40% on internal membranes, and 41% in the cytosol. For simulated Δ*rdi1* cells we found that 67% of all Cdc42 was distributed to internal membranes and 33% to the plasma membrane. For control cells we found 20% on the plasma membrane, 40% in the cytosol, and 40% on internal membranes.

The results shown in Fig. 4-7 were obtained from 400 runs for each point in parameter space, with the same simulation time and evaluation procedure as described for fitting the model above. Model parameters used in simulations are summarized in **Supplementary Table S9**.

Robustness of polarization dynamics. The GDI-dependent polarization pathway alone can be described in terms of deterministic dynamics by a set of partial differential equations. This set of reaction-diffusion equations allows growth of a small perturbation of the unpolarized state and hence pattern formation. Our stochastic simulations of this pathway show that only one stable cluster is established. We address this behavior to the Cdc42 number conservation similar to other mass conserved polarity models[28, 66]. To check for robustness of this behavior against parameter variations we changed each reaction rate separately between 1/2 and twice its control cell value and found that either a single stable polarity cluster was formed at the end of the simulations or that in some cases the polarization efficiency was lost as for example for a higher hydrolysis rate (Fig. 6a). This analysis showed that the formation of a single stable polarity cluster opposed to multiple stable clusters is indeed a robust property of GDI-mediated polarization.

The actin-dependent polarization pathway alone is prone to production of multiple caps as there is always the possibility that actin bundles nucleate at two (or more) distant sites on the plasma membrane. However, the risk to form two distant polarization sites can be decreased by a reduction of the probability for actin bundle nucleation. This reduction provides the polarization site which is established first with more time to redistribute Cdc42 on the membrane and therefore enhances the probability to nucleate the second actin bundle in close vicinity to the first one. The actin bundle nucleation rate is given by the product of the local Cdc42-GTP concentration times rate constant *e*. Hence, a change of the hydrolysis rate allows to vary the probability for actin bundle nucleation. Indeed, we found that the number of double caps in simulated Δ*rdi1* cells is reduced at higher hydrolysis rates as can be seen in Fig. 7c. Once formed clusters of this polarization pathway are stable as we assumed an irreversible actin bundle nucleation. To test for robustness of the ability to form multiple clusters we changed each reaction rate of the actin-dependent polarization pathway separately between 1/2 and twice its control cell value. We found that the risk to form two stable clusters did not vanish in most cases. However, for some changes we found that the number of double caps was strongly reduced, e.g. for a higher hydrolysis rate as can be seen in Fig. 7c. These observations were accompanied by a simultaneous reduction of the general polarization efficiency (e.g. compare Fig. 6a, 7c) and arise due to an insufficient probability to reliably

nucleate one or even two actin bundles in all cells within the simulation time of ~20 minutes. We concluded that the ability to occasionally form multiple stable clusters is a robust property of actin-dependent polarization as long as the polarization sites are established at all.

To check the robustness of unique control cell polarization we combined both polarization pathways and varied each model reaction rate separately between 1/2 and twice its control cell value. We found that the occurrence of multiple stable polarity clusters was inhibited or at least significantly reduced compared to the corresponding findings for the actin-dependent polarization pathway alone. Hence, the ability of control cells to suppress the establishment of multiple stable caps compared to Δ*rdi1* cells is a robust model property. Stronger parameter changes are necessary to weaken this ability as for example shown in Fig. 7c for different hydrolysis rates. In this case we observed that the occurring multiple clusters were stable and localized together with the actin bundles indicating that the stability of multiple clusters arises from the actin part of the model. The influence of the parameter variations is summarized in **Supplementary Fig. S4**.

Test of previous polarization model. To experimentally verify the polarization model proposed by Goryachev and Pokhilko we considered the GEF Cdc24 dynamics predicted by this model. The model assumed that cytosolic Bem1-Cdc24 complexes (E_c) can attach to the membrane with a basal rate k_1 or attach by forming a complex M with Cdc42-GTP (T) on the membrane with rate k_7. Membrane-bound Bem1-Cdc24 (E_m) was allowed to detach with rate k_{-1} or to form a complex with Cdc42-GTP with rate k_4. The opposite reaction of the complex formation was included with rate k_{-4}.

Given these reactions we concluded that for very low Cdc42-GTP concentrations all Bem1-Cdc24 on the membrane will be given in its Cdc42-GTP independent form E_m. In contrast, for high Cdc42-GTP concentrations the reactions k_7 and k_4 will strongly enhance the formation of M complexes on the expense of E_m and E_c. Therefore, the fraction of Cdc24 on the membrane, which can detach to the cytosol with rate k_{-1}, gets smaller at higher Cdc42-GTP concentrations.

In general, the time scale at which Cdc24 is removed from a membrane compartment is given by the fraction of the total Cdc24 number and the protein flux J_- out of this compartment, i.e. $t = (\grave{O}E_m + \grave{O}M)/J_-$. Neglecting the contribution of the small lateral membrane diffusion the time τ is given by

$$t = \frac{\partial E_m + \partial M}{k_{-1}\partial E_m}.$$

Hence, given the aforementioned dependence of M and E_m on Cdc42-GTP the model predicts that time τ depends on the concentration of Cdc42-GTP as well. To obtain a more quantitative expression for τ we used approximate expressions for E_m and M derived by Goryachev and Pokhilko assuming rapid cytosolic diffusion, fast reaction kinetics compared to the membrane diffusion, and separation of time scales. These expressions are given by

$$E_m = E_c(\frac{k_1}{k_{-1}} + \frac{k_7}{k_{-1}}T) \text{ and } M = E_c T(\frac{k_4 k_7}{k_{-4}k_{-1}}T + \frac{k_4 k_1}{k_{-4}k_{-1}} + \frac{k_7}{k_{-4}})$$

where E_c is assumed to be constant due to rapid cytosolic diffusion. The term of M with quadratic dependence on T represents the core reaction necessary for the Turing model. Using the parameters given by the authors we obtained[28, 46].

$$E_m = E_c(1+\frac{T}{\mu M}) \text{ and } M = E_c\frac{T}{\mu M}(2+\frac{T}{\mu M}).$$

Accordingly, for the exchange time τ of Cdc24 we obtained

$$t = \frac{\partial(1+\frac{T}{\mu M}) + \partial\frac{T}{\mu M}(2+\frac{T}{\mu M})}{k_{-1}\partial(1+\frac{T}{\mu M})}.$$

Note that the concentration of membrane-bound proteins is measured per volume in a 10 nm thick layer along the membrane[28]. Again we found that τ depends on the concentration of active Cdc42. The time τ can approximately be determined using fluorescence recovery after photobleaching (FRAP) of Cdc24. Importantly, we found that the FRAP time of polarized Cdc24 did not change as we reduced the Cdc42 hydrolysis by deletion of GAP Bem2 (**Supplementary Fig. S3B**) indicating that τ is not affected by changes of Cdc42-GTP concentrations. According to the model by Goryachev τ is only insensitive to changes in Cdc42-GTP concentration if $T \ll 1\mu M$ in the cluster. However, this condition implies that $M \ll E_m$, $M \sim T$ and $E_m = const$. Hence, the model by Goryachev implies that the Cdc24 FRAP rate is only unaffected by changes of Cdc42 hydrolysis if the total Cdc24 $E_m + M$ is almost homogenously distributed along the membrane. This clearly contradicts experiments showing that Cdc24 accumulates at the polarization site[14].

4. Supplementary References

60. Gulli, M.P. *et al.* Phosphorylation of the Cdc42 exchange factor Cdc24 by the PAK-like kinase Cla4 may regulate polarized growth in yeast. *Mol Cell* **6**, 1155-1167 (2000).
61. Gillespie, D.T. Exact stochastic simulation of coupled chemical reactions. *The Journal of Physical Chemistry* **81**, 2340-2361 (1977).
62. Bernstein, D. Simulating mesoscopic reaction-diffusion systems using the Gillespie algorithm. *Phys Rev E Stat Nonlin Soft Matter Phys* **71**, 041103 (2005).
63. Zheng, Y., Cerione, R. & Bender, A. Control of the yeast bud-site assembly GTPase Cdc42. Catalysis of guanine nucleotide exchange by Cdc24 and stimulation of GTPase activity by Bem3. *J Biol Chem* **269**, 2369-2372 (1994).
64. Ghaemmaghami, S. *et al.* Global analysis of protein expression in yeast. *Nature* **425**, 737-741 (2003).
65. Shimada, Y., Gulli, M.P. & Peter, M. Nuclear sequestration of the exchange factor Cdc24 by Far1 regulates cell polarity during yeast mating. *Nat Cell Biol* **2**, 117-124 (2000).
66. Otsuji, M. *et al.* A mass conserved reaction-diffusion system captures properties of cell polarity. *PLoS Comput Biol* **3**, e108 (2007).